JCI The Journal of Clinical Investigation

MAP3K1 mutations confer tumor immune heterogeneity in hormone receptor-positive HER2-negative breast cancer

Yuwen Cai, … , Zhiming Shao, Ke-Da Yu

J Clin Invest. 2024. https://doi.org/10.1172/JCI183656.

Research In-Press Preview **Immunology** **Oncology**

Hormone receptor-positive (HR^+)/human epidermal growth factor receptor 2-negative ($HER2^-$) breast cancer, the most common type of breast cancer, is facing challenges such as endocrine therapy resistance and distant relapse. Immunotherapy has shown progress in treating triple-negative breast cancer, but immunological research on $HR^+/HER2^-$ breast cancer is still in its early stages. Here, we performed a multi-omics analysis of a large cohort of $HR^+/HER2^-$ breast cancer patients (n = 351) and revealed that $HR^+/HER2^-$ breast cancer possessed a highly heterogeneous tumor immune microenvironment. Notably, the immunological heterogeneity of $HR^+/HER2^-$ breast cancer was related to *MAP3K1* mutation and we validated experimentally that *MAP3K1* mutation could attenuate $CD8^+$ T cell-mediated antitumor immunity. Mechanistically, *MAP3K1* mutation suppressed MHC-I-mediated tumor antigen presentation through promoting the degradation of *antigen peptide transporter 1/2 (TAP1/2)*mRNAs, thereby driving tumor immune escape. In preclinical models, the postbiotics tyramine could reverse the *MAP3K1* mutation-induced MHC-I reduction, thereby augmenting the efficacy of immunotherapy. Collectively, our study identified the vital biomarker driving the immunological heterogeneity of $HR^+/HER2^-$ breast cancer and elucidated the underlying molecular mechanisms, which provided the promise of tyramine as a novel therapeutic strategy to enhance the efficacy of immunotherapy.

MAP3K1 mutations confer tumor immune heterogeneity in hormone receptor-positive HER2-negative breast cancer

Yu-Wen Cai[1, 2, #], Cui-Cui Liu[1, 2, #], Yan-Wu Zhang[3, #], Yi-Ming Liu[1, 2, #], Lie Chen[1, 2], Xin Xiong[1, 2], Zhi-Ming Shao[1, 2], Ke-Da Yu[1, 2, 4, *]

[#] The authors contributed equally to this work.

* Corresponding author

[1] Department of Breast Surgery, Fudan University Shanghai Cancer Center and Cancer Institute, Department of Oncology, Shanghai Medical College, Fudan University, Shanghai 200032, P.R. China

[2] Key Laboratory of Breast Cancer in Shanghai, Shanghai 200032, P.R. China

[3] Department of Breast Surgery. The Third Affiliated Hospital of Zhengzhou University, Zhengzhou, 450000, P.R. China.

[4] Lead Contact

[*]Correspondence to:

Ke-Da Yu, Department of Breast Surgery, Shanghai Cancer Center and Cancer Institute, Department of Oncology, Shanghai Medical College, Fudan University, Shanghai 200032, P. R. China; Tel: +(86)18017317597; E-mail: yukeda@fudan.edu.cn (K.D.Y.)

Conflict-of-interest statement:

The authors have declared that no conflict of interest exists.

Abstract

Hormone receptor-positive (HR^+)/human epidermal growth factor receptor 2-negative ($HER2^-$) breast cancer, the most common type of breast cancer, is facing challenges such as endocrine therapy resistance and distant relapse. Immunotherapy has shown progress in treating triple-negative breast cancer, but immunological research on $HR^+/HER2^-$ breast cancer is still in its early stages. Here, we performed a multi-omics analysis of a large cohort of $HR^+/HER2^-$ breast cancer patients (n = 351) and revealed that $HR^+/HER2^-$ breast cancer possessed a highly heterogeneous tumor immune microenvironment. Notably, the immunological heterogeneity of $HR^+/HER2^-$ breast cancer was related to *MAP3K1* mutation and we validated experimentally that *MAP3K1* mutation could attenuate $CD8^+$ T cell-mediated antitumor immunity. Mechanistically, *MAP3K1* mutation suppressed MHC-I-mediated tumor antigen presentation through promoting the degradation of *antigen peptide transporter 1/2* (*TAP1*/*2*) mRNAs, thereby driving tumor immune escape. In preclinical models, the postbiotics tyramine could reverse the *MAP3K1* mutation-induced MHC-I reduction, thereby augmenting the efficacy of immunotherapy. Collectively, our study identified the vital biomarker driving the immunological heterogeneity of $HR^+/HER2^-$ breast cancer and elucidated the underlying molecular mechanisms, which provided the promise of tyramine as a novel therapeutic strategy to enhance the efficacy of immunotherapy.

Keywords: $HR^+/HER2^-$ breast cancer; immunological heterogeneity; *MAP3K1* mutation; MHC-I; postbiotics tyramine

Introduction

Breast cancer is the most common female cancer worldwide. Hormone receptor-positive [HR^+, defined as positive estrogen receptor (ER) and/or positive progesterone receptor (PR) status] and human epidermal growth factor receptor 2-negative ($HER2^-$) breast cancer accounts for 65-75% of all breast cancers, for which endocrine therapy is the standard-of-care (1). Although $HR^+/HER2^-$ breast cancer is highly endocrine responsive, resistance to endocrine therapy is common (2) and the risk of recurrence and death from breast cancer persists for over 20 years after original diagnosis (3). New approaches, including novel therapies and combination treatments, are therefore urgently needed to refine and improve the treatment strategies for this population.

Over the past few years, immunotherapy has shown great promise in multiple tumor types, such as melanoma, non-small cell lung cancer and triple-negative breast cancer (TNBC). Immune checkpoint inhibitors (ICIs) have benefited TNBC patients, with the relevant fundamental research and clinical transformation being well-established. However, the therapeutic exploration of ICIs in $HR^+/HER2^-$ breast cancer is still in its early stages. Phase I-II clinical studies with small sample size, such as GIADA (NCT04659551) (4), KEYNOTE-028 (NCT02054806) (5), NCT02779751 (6), NCT03051659 (7) and so on (8), provided the preliminary efficacy and safety data of ICIs in $HR^+/HER2^-$ breast cancer. I-SPY2 study suggested that there was a significantly higher pathologic complete response (pCR) rate in patients received ICIs treatment than those received neoadjuvant chemotherapy alone (9, 10). Recent large phase III clinical studies, KEYNOTE-756 (NCT03725059, n = 1278) and CheckMate-7FL

(NCT04109066, n = 510), showed that ICIs group could significantly improve the pCR rate compared with the control group, which confirmed the prospect of immunotherapy in treating $HR^+/HER2^-$ breast cancer. Notably, the pCR rate is generally 20% in $HR^+/HER2^-$ breast cancer, which is far less than 50% in TNBC. Moreover, the subgroup analyses in the two large trials indicated that pCR rate varied from 5% to 50% in different subgroups, suggesting that $HR^+/HER2^-$ breast cancer possessed a highly heterogeneous tumor immune microenvironment. Therefore, we need to identify the key biomarkers of immune heterogeneity and further dissect the biological mechanisms underlying the immunological resistance, so as to develop novel, tailored treatment strategies to enhance immunotherapy efficacy in treating $HR^+/HER2^-$ breast cancer.

Here, we performed a comprehensive analysis of the clinical, genomic, and transcriptomic data of $HR^+/HER2^-$ breast cancers (n = 351) in the Chinese Breast Cancer Genome Atlas (CBCGA) cohort as we previously reported (11) and revealed that there were two immunologically heterogeneous phenotypes. Notably, the immunosuppressive phenotype was associated with a high prevalence of *MAP3K1* mutation, which suppressed MHC-I-mediated tumor antigen presentation by promoting the degradation of *antigen peptide transporter 1/2* (*TAP1/2*) mRNAs, and thus reshaped the tumor immune microenvironment of $HR^+/HER2^-$ breast cancers.

Results

MAP3K1 mutation is closely correlated with immune microenvironment heterogeneity in $HR^+/HER2^-$ breast cancer

To explore the heterogeneity of $HR^+/HER2^-$ breast cancer immune microenvironment, we performed the multi-omics analysis with our CBCGA cohort (Figure 1A). First, we employed the Microenvironment Cell Populations-counter (MCP-counter) analysis to depict the microenvironment features of $HR^+/HER2^-$ breast tumors. The results of NbClust analysis showed that two was the optimal and stable clustering number (Supplemental Figure 1A). Then, we performed the Partitioning Around Medoid (PAM) clustering analysis and classified the $HR^+/HER2^-$ breast cancers into two subtypes, namely immune-hot (IHot, characterized by a relatively high immune cell and low stromal cell infiltration level) and immune-cold (ICold, characterized by a converse landscape) (Figure 1B and Supplemental Figure 1B). For the ICold subtype, we considered that the low infiltration level of immune cell in partial tumors is attributed to the relatively benign nature, which is associated with a good prognosis in clinic. We therefore discarded patients who had been followed up for over 10 years and still survived in the ICold subtype (Supplemental Table 1). The remaining ICold patients were subjected to further analysis.

As expected, the tumor mutation burden (TMB) and ki-67 index/*MKI67* mRNA expression in the ICold subtype were comparable to or higher than that in the IHot subtype (Figure 1, C and D, and Supplemental Figure 1, C and D). However, there was a lower *CD274* (the gene encoding PD-L1) mRNA expression in the ICold than IHot

subtype (Figure 1E and Supplemental Figure 1E). To further explore whether they have varying response to immunotherapy, we then extrapolated the two subtypes to I-SPY2 (9, 10), a neoadjuvant platform trial, and discovered that both in the arms receiving anti-PD-L1 or anti-programmed death-1 (PD-1) treatment, ICold subtype achieved a significantly lower pCR rate than IHot subtype (Figure 1, F and G). In summary, we revealed two immunologically distinct subtypes in terms of immune infiltration, PD-L1 expression, and response to immunotherapy with comparable TMB and clinical features, indicating that $HR^+/HER2^-$ breast cancer possessed a highly heterogeneous immune environment.

Then, we further explored the pivotal biomarkers contributing to the immune microenvironment heterogeneity in $HR^+/HER2^-$ breast cancers. We depicted the nonsynonymous somatic mutation landscape of tumors in CBCGA cohort (Figure 1H) and compared the mutation prevalence of cancer-related genes between the ICold and IHot subtypes in CBCGA, TCGA and METABRIC cohorts (Supplemental Figure 1F). Intersect of the results from three cohorts revealed two candidate genes: *TP53* and *MAP3K1* (Figure 1I). Previous studies have demonstrated the important role of p53 in regulating antitumor immunity (12-14), which confirmed the reliability of our analyses. MEKK1, the gene product of *MAP3K1*, is a 196-kDa serine-threonine kinase in the MAPK family with functions in cell viability, apoptosis and cell motility/migration in multiple normal and tumor cell types. It has never been reported that there was an association between *MAP3K1* mutations and the efficacy of anti-tumor immunotherapy, which triggered our great interest. To further explore the function of *MAP3K1* mutation

on regulating tumor immune microenvironment, we performed the Cell-type Identification by Estimating Relative Subsets of RNA Transcripts (CIBERSORT) analysis and discovered that tumors with *MAP3K1* mutation had a lower abundance of $CD8^+$ T cells, the main immune effector cells for anti-tumor immunity, compared to tumors without *MAP3K1* mutation (Figure 1J). Moreover, tumors with *MAP3K1* mutation also had a significantly lower mRNA expression of *GZMA*, a cytotoxicity marker of T cells (Figure 1K). These results indicated that *MAP3K1* gene was closely correlated with immune heterogeneity in $HR^+/HER2^-$ breast cancer and its mutation could induce an immunosuppressive microenvironment.

Map3k1-mutant tumors evade $CD8^+$ T cell-mediated immunity in vivo

MEKK1, the gene product of *MAP3K1*, consists of a RING zinc finger domain near the N-terminus and a serine/threonine kinase domain at the C-terminus. We observed that a majority of *MAP3K1* mutation in the patient cohort was truncated, resulting the loss of the kinase domain of MEKK1 (Figure 2A). To further investigate the effect of *MAP3K1* mutation on tumor progression, we knocked out its endogenous expression and then overexpressed either *Map3k1* WT or C-terminus kinase domain-truncated mutant (Mut) in murine luminal breast cancer cell lines 67NR and EMT6. The KO efficacy (Supplemental Figure 2A) and overexpression efficacy (Supplemental Figure 2B) were confirmed by western blot, respectively.

We first assessed the effect of *Map3k1* gene itself on cancer cell and discovered that *Map3k1*-WT significantly promoted cell proliferation in vitro, which is consistent

with previously reported researches (15-17), while *Map3k1*-mut abolished this promoting effect (Supplemental Figure 2C). Data from METABRIC cohort also indicated a lower *MKI67* mRNA expression in tumors with *MAP3K1* mutation (Supplemental Figure 2D). With the above mutation model, we also employed an orthotopic mammary xenograft model in BALB/c mice. Interestingly, *Map3k1*-WT inhibited the tumor growth but *Map3k1*-Mut displayed the opposite effect on tumor growth in vivo (Figure 2, B and C, and Supplemental Figure 2, E and F). These results indicated that the tumor immune microenvironment could be responsible for the inconsistency effect of *Map3k1* in vivo and in vitro.

To validate our speculation, we therefore isolated tumors from mice and analyzed the microenvironment characteristics. As expected, we found a reduced proportion and inhibited function of $CD8^+$ T cells in *Map3k1*-Mut tumors (Figure 2, D-G and Supplemental Figure 2, G-J), which might explain the faster tumor progression of *Map3k1*-Mut tumors compared to *Map3k1*-WT tumors in vivo. To further confirm the necessity of $CD8^+$ T cell-mediated tumor immunity in *Map3k1*-modulated tumor growth, we used a CD8 neutralizing antibody to deplete $CD8^+$ T cells in mice (Supplemental Figure 3, A and B). We observed that depletion of $CD8^+$ T cells abolished the growth difference among tumors with varying *Map3k1* mutation status (Supplemental Figure 3, C and D), indicating the critical role of $CD8^+$ T cells in mediating the effects of *Map3k1* on tumor growth in vivo.

Map3k1-mutant tumor cells suppress $CD8^+$ T cell-mediated immunity in vitro

To test whether *Map3k1* status in tumor cells can directly impact the function of $CD8^+$ T cells in vitro, we generated 67NR and EMT6 cell lines with varying *Map3k1* status and stably presenting a chicken ovalbumin peptide ($OVA_{257-264}$). We then constructed an in vitro coculture system by coculturing these OVA-expressing cell lines and splenocytes isolated from an OT-I transgenic mouse, the $CD8^+$ T cells of which can specifically recognize the $OVA_{257-264}$ antigen in the context of MHC-I allele $H\text{-}2K^b$ (18), and thus elicit strong epitope-specific immune responses (Figure 3A). To confirm the reliability of our findings regarding the function of *Map3k1* mutation, we also constructed another high-frequency mutant (Mut': MEKK1-$K1037R^{fs*4}$ mutant, which possessed high mutation rate in the CBCGA cohort) for the vitro experiments.

In the coculture system, we discovered a significantly reduced proportion of cytokines interferon-γ (IFNγ)-positive $CD8^+$ and tumor necrosis factor-α (TNFα)-positive $CD8^+$ T cells (Figure 3, B and C, and Supplemental Figure 4, A and B), consistent with a markedly reduced levels of cytokines IFNγ and TNFα in *Map3k1*-Mut/Mut' groups compared to *Map3k1*-WT group (Figure 3, D and E, and Supplemental Figure 4, C and D). The reduced cytotoxicity of $CD8^+$ T cells in the coculture system induced by *Map3k1*-Mut/Mut' tumor cells was confirmed by lactate dehydrogenase (LDH) assay (Figure 3F and Supplemental Figure 4E). In line with these findings, we also discovered that *Map3k1*-Mut/Mut' tumor cells had a significantly lower percentage of dead tumor cells in the coculture system (Figure 3G and Supplemental Figure 4F). Overall, these findings suggest that *Map3k1*-Mut/Mut' tumor cells have an enhanced ability to evade killing by $CD8^+$ T cells in vitro.

Map3k1 mutation inhibits tumor antigen presentation

To reveal the mechanism underlying *Map3k1* mutation mediated immune evasion, we collected *Map3k1*-WT/*Map3k1*-Mut tumors isolated from mice, as mentioned above, for RNA-Seq. Enrichment analysis on the RNA-Seq data demonstrated several immune-related pathways downregulated in *Map3k1*-Mut tumors compared to *Map3k1*-WT tumors, among which the MHC-I mediated antigen presentation pathway (GO: 0019885) might directly explain the findings we had observed (Figure 4A). The downregulation of the MHC-I mediated antigen presentation pathway in patients with *MAP3K1* mutation was also observed in the METABRIC cohort (Supplemental Figure 5A). To confirm the effect of *Map3k1* on this pathway, we performed the in vitro coculture assay again and collected tumor cells to measure the surface expression of MHC-I and OVA antigen. As a result, we observed less presentation of MHC-I and OVA antigen in *Map3k1*-Mut tumor cells compared to *Map3k1*-WT group using flow cytometry (Figure 4, B and C), in line with the weaker MHC-I fluorescence intensity observed on the surface of *Map3k1*-Mut tumor cells (Figure 4D and Supplemental Figure 5B).

We then focused on the downregulated genes in the antigen presentation pathway to determine which step in antigen presentation was suppressed by *Map3k1* mutation (Figure 4E). Among the downregulated genes in the RNA-Seq data of mouse tumors, *TAP1* and *TAP2* were also found to have a lower mRNA expression in patients with *MAP3K1* mutation compared to those without in both TCGA and METABRIC cohorts

(Figure 4, F and G). However, there was no significant difference in the expression of *HLA-A*, the homologous gene of the other downregulated genes in mouse data, between patients with and without *MAP3K1* mutation (Supplemental Figure 5C). We then confirmed the downregulation of TAP1/2 expression in *Map3k1*-Mut cancer cells compared to *Map3k1*-WT cancer cells in the coculture system by quantitative PCR with reverse transcription (RT–qPCR) analysis and western blot assay (Supplemental Figure 6, A and B). These results displayed that *MAP3K1* mutation could inhibit *TAP1* and *TAP2* expression to disturb the endogenous antigen presentation.

To further determine whether *Map3k1* regulated surface MHC-I expression via regulating *Tap1*/*2* expression, we performed rescue assay by overexpressing *Tap1*/*2 in Map3k1*-mut tumor cells. In the coculture system, we found transient overexpression of *Tap1*/*2* could efficiently rescue the downregulation of MHC-I expression in tumor cell surface and the reduced proportions of $IFN\gamma^{+}CD8^{+}$ and $TNF\alpha^{+}CD8^{+}$ T cells in OT-I splenocytes induced by *Map3k1* mutation (Supplemental Figure 6, C and D, and Supplemental Figure 6, E-H), which validated the key role of *Tap1/2* in the modulation of tumor antigen presentation effected by *Map3k1*.

Map3k1 **mutation destabilizes** ***Tap1*****/*****2*** **mRNAs**

We then investigated how *Map3k1* mutation downregulated *Tap1*/*2* expression. Initially, we explored whether *Map3k1* could regulate the transcription level of *Tap1*/*2*. We performed the RT-qPCR analysis but observed no significant difference in the pre-mature *Tap1*/*2* expression between *Map3k1*-WT and *Map3k1*-Mut tumor cells in

coculture with splenocytes from OT-I mice, indicating that *Map3k1* might regulate *Tap1*/*2* expression in a post-transcription manner (Figure 5A). We then tested the stability of *Tap1*/*2* mRNA in tumor cells in the coculture system. In summary, we treated the coculture system with 10 μg ml^{-1} actinomycin D, and collected tumor cells at 4 and 8 hours after treatment, respectively, for RT-qPCR analysis. We observed that compared to *Map3k1*-WT, *Map3k1*-Mut could significantly promote *Tap1*/*2* mRNAs degradation in tumor cells (Figure 5B). Considering that MEKK1 is not an RNA binding protein (RBP), we speculated that MEKK1 could destabilize *Tap1*/*2* mRNAs through another molecule, which could bind and degrade *Tap1*/*2* mRNAs (Supplemental Figure 7A).

We therefore performed RNA pull-down and IP assays to identify RBPs that could bind *Tap1*/*2* mRNA and proteins that interacted with MEKK1, respectively. We focused on intersect of the proteins identified in the two assays (Supplemental Figure 7B), among which DEAD box helicase 17 (DDX17) triggered our interest. DDX17 is an RNA helicase that had been reported to be widely involved in RNA metabolism (19, 20). We confirmed the direct binding of *Tap1*/*2* RNA to DDX17 by RNA pull-down (Figure 5C), and we also observed less binding of *Map3k1*-Mut to DDX17 compared with *Map3k1*-WT by IP assay (Figure 5D). In addition, we performed an RNA immunoprecipitation (RIP) assay to compare the ability of DDX17 to bind *Tap1*/*2* mRNAs in *Map3k1*-WT and *Map3k1*-Mut tumor cells in the coculture system. As a result, we found that compared to *Map3k1*-WT, *Map3k1*-Mut significantly attenuated the binding of DDX17 to *Tap1*/*2* mRNAs (Figure 5E). In summary, these results support

our speculation that, the binding of *Map3k1*-WT to DDX17 could weak the ability of DDX17 to bind and degrade *Tap1*/*2* mRNAs. *Map3k1*-Mut lost this effect, leading to promoted degradation of *Tap1*/*2* mRNAs in *Map3k1*-Mut compared to *Map3k1*-WT tumor cells.

We then performed rescue assays using a small interfering RNA targeting *Ddx17* (*siDdx17*). Tumor cells with varying *Map3k1* mutation status in the coculture system were transfected with *siDdx17* and then the actinomycin D treatment assay was performed again. We found that silencing *Ddx17* abolished the promoting effect of *Map3k1*-Mut on the *Tap1*/*2* mRNAs degradation (Figure 5F). Consistently, we observed comparable mRNA and protein levels of TAP1/2 between *Map3k1*-WT and *Map3k1*-Mut tumor cells in the coculture system after silencing *Ddx17* (Supplemental Figure 8, A and B). Moreover, we confirmed that silencing *Ddx17* could increase surface MHC-I and OVA antigen expression of *Map3k1*-Mut tumor cells as measured by both immunofluorescence (Supplemental Figure 8C) and flow cytometry (Supplemental Figure 8, D and E, and Supplemental Figure 9, A-D), and thus enhanced the activation of $CD8^+$ T cells in the coculture system. All these results indicated that MEKK1 mutation could inhibit its binding to DDX17 and thus promote DDX17-mediated degradation of *Tap1*/*2* mRNAs.

Tyramine augments the efficacy of immunotherapy in HR^+/$HER2^-$ breast cancer

As demonstrated above, *Map3k1* mutation could reshape the immune microenvironment by reducing the surface MHC-I expression to promote tumor growth.

We then attempted to hunt for strategies that can efficiently reverse the surface MHC-I downregulation. We noticed that recently, postbiotics released from *L. paracasei* (PB) was reported to induce a significant increase in surface MHC-I expression on several tumor types including breast cancer (21). We therefore tested the efficacy of the metabolites in the postbiotic mixture to upregulate surface MHC-I in our cell lines. As a result, we found metabolites tyramine (Tyra) and 3-hydroxy-3-methylglutarate (3-Hydr) could significantly upregulate surface MHC-I in both 67NR and EMT6 cell lines, while sucrose could not (Supplemental Figure 10, A-F). Considering the commonality of tyramine in daily life and therefore a better potential for clinical transformation, we then applied Tyra into the in vitro coculture system and found that Tyra could efficiently reverse the downregulation of surface MHC-I and OVA antigen in *Map3k1*-Mut tumor cells, and thus enhanced the activation of $CD8^+$ T cells in the coculture system (Supplemental Figure 10, G-J). At last, we investigated whether Tyra could augment the efficacy of anti-PD-1 immunotherapy in the mouse models.

We found that anti-PD-1 treatment alone achieved limited success in suppress tumor growth, while the combination of Tyra and anti-PD-1 treatment induced a strong tumor growth inhibition (Figure 6, A and B). Moreover, the analysis of flow cytometry on tumor tissues demonstrated that combination of Tyra and immunotherapy significantly increased the infiltration level (Figure 6C) and promoted the activation (Figure 6, D and E) of $CD8^+$ T cells. Taken together, the results that the combination of postbiotic Tyra with PD-1inhibitor could be a therapeutic strategy for the *MAP3K1* mutation subgroup in $HR^+/HER2^-$ breast cancers.

Discussion

Our multi-omics analysis of a large cohort of patients revealed that *MAP3K1* mutation was associated with an immunosuppressed microenvironment in $HR^+/HER2^-$ breast cancers. Administration of Tyra could reverse the downregulation of tumor antigen presentation caused by *MAP3K1* mutation, thus promoting $CD8^+$ T cell-mediated antitumor immunity and enhancing the efficacy of anti-PD-1 immunotherapy in $HR^+/HER2^-$ breast tumors in vivo.

Nowadays, certain progress has been made for immunotherapy in treating TNBC (22, 23), and FDA has approved pembrolizumab for this disease. However, immunotherapy has not yet been widely applied to $HR^+/HER2^-$ breast cancer, which accounts for 2/3 of all breast cancers. A key reason for this limited application is the lack of understanding regarding the factors contributing to the unresponsiveness of $HR^+/HER2^-$ breast cancer to immunotherapy. Here, we systematically revealed the immunological heterogeneity of a large cohort of $HR^+/HER2^-$ breast cancer patients (n = 351). This cohort had a nontreated baseline, and therefore, there is no treatment influence on the immune status. We discovered that the immunosuppressive tumor microenvironment was associated with a high prevalence of *MAP3K1* mutation, suggesting that *MAP3K1* plays an important role in mediating resistance to immunotherapy.

MAP3K1 is one of the most frequently mutated cancer genes in luminal breast cancer (24). Previous studies have demonstrated the functions of *MAP3K1* in promoting cell survival, invasion, and migration, etc. (15-17, 25-27). It should also be noted that

MAP3K1 is one of the nodes in MAPK-pathway. Although there is evidence that MAPK-pathway blockade such as MEK inhibitors could enhance anti-tumor immune responses (28, 29), little is known about whether and how *MAP3K1* itself modulate tumor microenvironment. There are also bioinformatics analyses indicating an association between *MAP3K1* mutation and an immunosuppressive tumor microenvironment (30-32), but evidence from experimental data is scarce and the underlying mechanisms remain elusive. In our study, we reported for the first time that *Map3k1* mutation could promote tumor growth through attenuating $CD8^+$ T cell-mediated antitumor immunity by downregulating tumor antigen presentation.

Although downregulation of MHC-I on tumor cells has been discovered early as one of the means of immune escape (33-35), no clear answer is yet available for how to overcome this obstacle in clinic (36). IFNγ is known to induce strong increases in surface MHC-I expression through the JAK-STAT pathway (37). However, the opposite effects and immunosuppressive functions (such as upregulating PD-L1 expression) of IFNγ has limited its clinical application (38). Recently, several novel strategies have been identified to specifically upregulate MHC-I expression, including gene perturbations targeting TRAF3 (39) and microbial metabolites (21), etc. Here, we demonstrated that postbiotics Tyra, the metabolite of *Lactobacillus paracasei*, could efficiently upregulate surface MHC-I expression and augment the efficacy of immunotherapy in $HR^+/HER2^-$ breast cancer. Given that postbiotics have been proven safe for human use, there is potential for rapidly translating Tyra into clinical practice, particularly in combination with existing immunotherapies.

Our study has some limitations. Since the prevalence of *MAP3K1* mutation in $HR^+/HER2^-$ breast cancer is less than 20%, the immunosuppressive tumor microenvironment cannot be entirely attributed to *MAP3K1* mutation. Whether other gene plays a role in the immune escape of $HR^+/HER2^-$ breast cancer, and whether *MAP3K1* can modulate the immunity in other cancer types remains unknown. In the mechanism part, we observed that *Map3k1*-WT could bind to DDX17 and thus weakens its ability to bind and degrade *Tap1/2* mRNAs. However, the specific binding sites between DDX17 and the other two molecules remains elusive. Moreover, how does the binding of *Map3k1*-WT reduce the degradation ability of DDX17, i.e., whether through inducing a conformational change of DDX17 or just be a competitively binding, still needs to be further explored.

In conclusion, our study demonstrated the ability of *MAP3K1* to modulate tumor microenvironment via regulating tumor antigen presentation and highlighted the clinical potential of postbiotics Tyra to enhance immunotherapy efficacy in $HR^+/HER2^-$ breast cancer.

Methods

Sex as a biological variable

Our study exclusively examined female mice because the disease modeled is only relevant in females.

Study cohorts

Our study included $HR^+/HER2^-$ breast cancer patients from a previously described cohort [CBCGA; 100% female, average age = 53 ± 11 years; 351 patients with RNA-Seq data, among whom 315 had whole exome sequencing (WES) data]. (11) TCGA (a total of 1,097 patients, 1.1% male and 98.9% female, average age = 58 ± 13 years; including 550 $HR^+/HER2^-$ breast cancer patients with RNA-Seq data, 0.9% male and 99.1% female, average age = 58 ± 13 years) and METABRIC (a total of 1985 patients, 100% female, average age = 61 ± 13 years; including 1222 $HR^+/HER2^-$ breast cancer patients with RNA-Seq data, 100% female, average age = 63 ± 12 years) cohorts were from the cBioPortal website (https://www.cbioportal.org/) and analyzed for external validation.

Cell lines

The mammary carcinoma cell line 67NR (gifted by Y. Kang Lab) was cultured in RPMI-1640 with 10% FBS, 2mM glutamine, and 100U penicillin/0.1mg ml^{-1} streptomycin. EMT6 cell line (Cat# CRL-2755) and human embryonic kidney cell line HEK293T (Cat# CRL-3216) were purchased from the American Type Culture

Collection and were cultured in DMEM containing 10% FBS, 2mM glutamine and 100U penicillin/0.1mg ml^{-1} streptomycin. Mycoplasma contamination was regularly monitored for all cell lines by the standard PCR method. Mouse splenocytes freshly isolated from OT-I mice were cultured in RPMI-1640 with 10% FBS, 1% HEPES, 1% sodium pyruvate, 0.05mM β-mercaptoethanol and 100U penicillin/0.1mg ml^{-1} streptomycin.

Animal studies

General

6–8-week-old female BALB/c mice were purchased from Charles River and housed at Shanghai Laboratory Animal Center under SPF conditions. Mice were housed in individually ventilated and pathogen-free cages with free access to water and a standard chow diet under the following conditions: 20-22℃ ambient temperature, 60±10% humidity, and 12 h light/darkness cycles. Mice health status was monitored through culture, serum and microscopic examination.

Tumor models

BALB/c mice were orthotopically injected with 1×10^6 67NR or EMT6 murine cells with varying *Map3k1* status. Once the tumors formed, tumor size was measured every three days using a caliper. Tumor volume (mm^3) was calculated by the following formula: $0.5 \times Length \times Width^2$.

Mouse treatments

Mice were treated with 400 µg Tyra in 40 µl DMSO or 40 µl DMSO alone in combination with anti-PD-1 (200 mg; BioXCell, Cat# BE0146) or its isotype control (200 mg; BioXCell, Cat# BE0089) upon tumors formation. For $CD8^+$ T cell depletion experiments, mice were treated weekly with 200 µg of CD8a depletion antibody (InvivoMAb anti-mouse CD8, BioXcell, Cat# BE0061) or its isotype control (InVivoMAb rat IgG2b isotype control, BioXcell, Cat# BE0090) for three weeks by intraperitoneal injection.

Method details

Estimation of immune and stromal cell numbers and unsupervised clustering

The Microenvironment Cell Populations-counter (MCP-counter) method was performed using the R package "MCPcounter" to quantify the absolute abundance of eight immune and two stromal cell populations from RNA-Seq data (40). Based on the MCP-counter results, we used R package "NbClust" to determine the best number of clusters (41) and then classified the samples using Partitioning Around Medoid (PAM) clustering ("pam" function in R package "cluster") into 2 clusters (42).

Mutation atlas

The WES data of each cohort was used to perform the mutation related analyses. The gene mutation rate in the ICold and IHot tumors was compared using a two-tailed Fisher's exact test to identify the ICold-specific mutated genes. "lollipopPlot" function

in R package “maftools” was used to generate the *MAP3K1* mutation atlas.

Extrapolation

We extrapolated our immune subtypes into the immunotherapy arm of I-SPY2 $HR^+/HER2^-$ breast cancer cohort using “pamr” package. Genes with standard deviation ranking in the top 80% were used for extrapolation. Before using the ‘‘pamr.train’’ and ‘‘pamr.predict’’ functions, the expression data was normalized using “scale” function in R.

CIBERSORT

The abundance of $CD8^+$ T cells in tumors was calculated the Cell-type Identification by Estimating Relative Subsets of RNA Transcripts (CIBERSORT) tool (https://cibersort.stanford.edu/) and then compared between the *MAP3K1*-WT and *MAP3K1*-Mut tumors (43).

Flow cytometry analysis

After in vivo experiments, mouse tumors were fully and quickly chopped using scalpel and digested in RPMI-1640 + 5% FBS + 2.5% HEPES + 100U penicillin/0.1mg ml^{-1} streptomycin + 200U ml^{-1} collagenase III (Sigma) at 37 ℃ with rotation for 60-90 min. Samples were then passed through a 70 μm cell strainer and then lysed with red blood cell lysis buffer (Solarbio, #R1010) for 5 min at room temperature. Then, the single-cell suspensions were washed in Cell Staining Buffer (BioLegend, Cat# 420201) and

were stained with Zombie Red™ Fixable Viability Kit (BioLegend, Cat# 423110; 1:1000 in DMSO) at 4 ℃ for 10 min, and then incubated with a monoclonal antibody against CD16/32 (BioLegend, Cat# 101320) at 4 ℃ for 10 min, and then incubated with the indicated flow antibodies at 4 ℃ for 30 min. All the flow cytometry antibodies are as follows: CD45 (clone 30-F11, BioLegend, Cat# 103107), CD3 (clone 17A2, BioLegend, Cat# 100222), CD8a (clone 53-6.7, BioLegend, Cat# 100708), Ep-CAM (clone G8.8, BioLegend, Cat# 118240), H-2K^b/H-2D^b (clone 28-8-6, BioLegend, Cat# 114619), IFNγ (clone XMG1.2, BioLegend, Cat# 505810), and TNFα (clone MP6-XT22, BioLegend, Cat# 506324). For intracellular staining of mouse IFNγ and TNFα, samples were stimulated with cocktail (Invitrogen, Cat# 00-4975-03) for 4 hours, fixed with fixation buffer (Invitrogen, Cat# 00-8222-49), permeabilized with Permeabilization buffer (Invitrogen, Cat# 00-8333-56), and then incubated with surface antibodies and finally intracellular antibodies to IFNγ and TNFα for 30 min at 4 ℃. A CytoFLEX software (Version 2.4.0.28, Beckman Coulter) and FlowJo software (Version 10.8.1, TreeStar) were used for further analyses.

Immunohistochemical staining

Sections were incubated with rabbit-anti-mouse CD8 antibody (Servicebio, Cat# GB15068, 1:400) overnight, stained with goat anti-rat IgG Ab (Servicebio, Cat# GB21303, 1:300) at room temperature for 50 min, and then counterstained with hematoxylin.

Enrichment analysis

For mouse RNA-Seq data, the student's t test was used to identify the Differentially Expressed Genes (DEGs), and GO enrichment analysis was performed using "enrichGO" function in R package "clusterProfile" based on DEGs. For human transcriptomic data in METABRIC cohort, "limma" package was used to perform the DEG analysis, and Gene set enrichment analysis (GSEA) was performed using the "gseGO" function.

Viral production and cell transfection

The CRISPR/Cas9 plasmids (MiaoLingBio, Cat# P51417) were cut using Esp3I enzyme (Thermo, Cat# FD0454), guided DNA targeting murine *Map3k1* (sequence listed in Supplemental Table 2) was then ligated to the plasmids. Overexpression plasmids (MiaoLingBio, Cat# P14038) encoding full-length *Map3k1* (WT) and kinase domain-truncated form (Mut) were generated through ECoRI and BamHI double enzyme cleavage. The authenticity was verified by sequencing. For coculture assays, OVA-expression plasmids (MiaoLingBio, Cat# P53920) were also used for transfection. All plasmids were packaged into viruses using HEK293T cells along with helper plasmids psPAX2 and pMD2.G and then transfected into cells. Infected cells were selected using puromycin (for KO transfection) and blasticidin (for *Map3k1* overexpression transfection). Cells were cultured for several generations between different transfections to restore cell viability.

Splenocyte isolation

OT-I mice were killed by carbon dioxide and spleens were collected on a cell strainer, crushed, and rinsed with serum-free RPMI-1640 medium. The filtrate was collected into 50-ml conical tubes and spun down at 1000 r.p.m. for 5min. Supernatant were removed and then the samples lysed with red blood cell lysis buffer (Solarbio, #R1010) for 5 min at room temperature. Samples were then spun down and resuspended in culture medium, counted and plated into the co-culture system.

Immune and tumor cell coculture assay

67NR-OVA/EMT6-OVA tumor cells with varying *Map3k1* status were seeded into plates in the culture medium listed above. Splenocytes were added into the coculture system once the tumor cells reached 50% confluency at a 10:1 ratio (immune cell:tumor cells). The culture medium and cells were collected for further experiments after 24 hours of coculture.

ELISA

Culture medium was collected from OT-I and tumor cell coculture system and the concentration of IFNγ and TNFα was measure by the Mouse IFNγ (Abcam, Cat# ab282274) and TNFα (Abcam, Cat# ab208348) ELISA Kits according to the manufacturer's instructions.

RT–qPCR analyses

The FastPure Cell/Tissue Total RNA Isolation Kit V2 (Nanjing Vazyme Biotech, Cat# RC112-01) was used to isolate the total RNA from tumor tissues or cells according to the manufacturer's instructions. RNA was reverse transcribed into cDNA with the HiScript II 1st Strand cDNA Synthesis Kit (Vazyme, China, Nanjing). Taq Pro Universal SYBR qPCR Master Mix (Vazyme, China, Nanjing) was used to perform the RT-qPCR assay. All the primers and their sequences are listed in Supplemental Table 2. All experiments were repeated for at least 3 times.

IP and mass spectrometry

67NR-OVA tumors cells with varying *Map3k1* status were collected for IP assay after coculture with OT-I splenocytes for 24 hours. Samples were lysed with IP/CoIP Kit (Absin, Cat# abs955) according to the manufacturer's instructions. Samples were incubated with FLAG antibodies (Cell Signaling Technology, Cat# 70586) at 4 °C for 5 hours and then denatured in 5x loading buffer containing SDS in boiling water for 10 minutes. Boiled samples were used for western blot or mass spectrometry. For mass spectrometry, we decolorized and washed the gels containing samples to make it transparent. Gels were freeze-dried and samples were reduced of disulfide bonds by dithiothreitol, alkylated, and then enzymatically hydrolyzed. Peptide segment was extracted and dried in vacuum. At last, samples were desalinated and the supernatant was added to the sample bottle for mass spectrometry (Q-extraction) detection.

RIP

After 24 hours of coculture, 67NR-OVA tumors cells with varying *Map3k1* status were collected for RIP assay using an RIP kit (Fitgene, Cat# FI88707) according to the manufacturer's instructions. In brief, 2×10^7 tumor cells were lysed in 500 µl of RIP lysis buffer for 30 min on ice. Samples were then centrifuged at 12,000 r.p.m. for 15 min at 4 °C. 30 µl of supernatant was collected as protein input and another 30 µl of supernatant was collected as RNA input. The rest supernatant was incubated with DDX17 antibodies (Proteintech, Cat# 19910-1-AP) at room temperature for 2 hours. 40 µl washed resin was added into each sample and incubated at 4 °C for 2 hours. Samples were washed for 3 times using lysis buffer. At the last wash, 100 µl of the supernatant was collected for western blot (tube A), and the rest 400 µl of the supernatant was collected for RNA isolation (tube B). Both tubes were centrifuged at 12,000 r.p.m. for 5 min at 4 °C, and supernatant was removed. For tube A, 20 µl 2 × loading buffer was added and samples were boiled for 3 min and then stored at -80 °C. For tube B, 40 µl of elution buffer was added and samples were eluted at room temperature for 10 min, and then centrifuged at 12,000 r.p.m. for 5 min, supernatant was collected and RNA was isolated using the method listed above.

RNA pull-down

RNA pull-down assay was then performed using a PureBinding RNA-Protein pull-down Kit (GENESEED, Cat# P0202). In brief, a total of 1×10^7 tumor cells were lysed in Capture Buffer supplemented with sufficient protease inhibitors and RNase inhibitors at 4 °C for 10 min. Samples were centrifuged at 13,000 r.p.m. for 10 min at

4 °C, 50 μl of supernatant were collected as input, and the rest of supernatant was used for further experiment. In the meantime, 50μl of Streptavidin Magnetic Beads for each sample was washed by Wash Buffer in a new 1.5mL centrifuge tube and then added with 50 pmol *Tap1*/*2* RNA probe, or 2 μl of negative RNA probe (contained in the kit). *Tap1*/*2* mRNAs were obtained through in vitro transcription using RiboTM RNAmax-T7 biotin labeled in vitro transcription kit (RIBOBIO, Cat# C11002-1) and negative RNA probe was included in the RNA pull-down kit. The mix was incubated at 4 °C with rotation for 30 min, and then washed by Wash Buffer. The supernatant was then divided equally into the mix, and was incubated at 4 °C with rotation for 1 hour. Samples were washed by Wash Buffer 5 times. At the last wash, supernatant was removed and the potein was used for western blot or mass spectrometry.

Western blotting

Total protein in cells was extracted and lysed in modified RIPA Lysis Buffer (Beyotime Biotech, Cat# P0013C) added with protease inhibitors (Beyotime Biotech, Cat# ST506). Protein concentrations were measured by BCA protein assay reagent (Yeasen, Cat# 20201ES90). Cellular proteins were separated by 10% SDS-PAGE and then transferred to PVDF membranes (Millipore, Cat# IPVH00010). The membranes were incubated with the indicated primary antibodies, and the corresponding signals were detected by an enhanced chemiluminescent substrate kit (Yeasen, #36208ES76). Proteins with similar molecular weights (TAP1 and TAP2) were detected by two repeated experiments and incubation separately.

Colony-formation assay

A total of 1,000 67NR/EMT6 tumor cells with varying *Map3k1* status were plated into 6-well plates in the culture medium listed above. After 7 days of culture, we removed the culture medium and rinsed the pates with PBS three times. Samples were then stained with Crystal Violet Staining Solution (Beyotime Biotech, Cat# C0121) at room temperature in darkness for 1 hour. Staining solution were then removed. Samples were washed by PBS three times and then images were captured.

Immunofluorescence

1×10^5 67NR/EMT6 tumor cells with varying *Map3k1* status receiving the indicated treatment or not were plated on sterile slides in 24-well plates. Samples were fixed in 4% PFA for 10 min, blocked in 5% bovine serum albumin (BSA, Solarbio, Cat# A8010) for 1 hour, incubated with MHC-I Antibody (Affinity, Cat# DF8558) at 4 °C overnight. Samples were washed with PBS 3 times before each step. The next day, samples were washed with PBS and then incubated with 594-conjugated Goat anti-Rabbit IgG (H+L) (ABclonal, Cat# AS039, 1:200, diluted by 0.1% BSA) at room temperature for 1 hour. Samples were then washed again and were dripped with Antifade Mounting Medium with DAPI (Beyotime Biotech, Cat# P0131). Sections were scanned with a Leica SP5 fluorescence confocal microscope 20× objective (Leica). All images were analyzed using an ImageJ software (Version 2.3.0).

Cytotoxicity assays

The CytoTox 96 Non-Radioactive Cytotoxicity Assay kit (Promega, Cat# G1780) was used to measure the cell lysis according to manufacturer's instructions.

Statistical analysis

In the multi-omics analysis of $HR^+/HER2^-$ breast cancer cohorts, Kolmogorov-Smirnov normality test was performed to test the data distribution. Continuous variables with non-normal distribution were compared using the Mann-Whitney Wilcoxon test. Categorical variables were compared using chi-square for trend test and Fisher's exact test. For the in vitro and in vivo experiments, one-way ANOVA with Tukey's test was used for three or more group-comparisons. The time-course of tumor volume was compared using Two-way ANOVA with Tukey's test. All analyses were performed in Graphpad Prism Software (version 8.4.2). *P* values, sample size, and the specific tests can be found in the corresponding figure legends. A *P* value less than 0.05 was considered significant.

Study approval

All human tissue samples in the CBCGA cohort were obtained after approval of the research by the FUSCC Ethics Committee, and each patient provided written informed consent for data and tissue use. All animal experiment protocols were approved by the Institutional Animal Care and Use Committee of Shanghai Laboratory Animal Center.

Data availability

The RNA-Seq and WES data of the CBCGA cohort can be viewed in the Genome Sequence Archive (GSA) database under accession codes PRJCA017539 (https://ngdc.cncb.ac.cn/bioproject/browse/PRJCA017539). The TCGA and METABRIC were downloaded from the cBioPortal website (https://www.cbioportal.org/). Mass spectrometry-quantified protein data are provided with this paper (Supplemental Table 3 and Supplemental Table 4). The mouse RNA-seq data has been deposited in the NCBI Gene Expression Omnibus (GEO: GSE276527).

This study did not report new original code. Any additional information required to reanalyze the data reported in this paper is available from the lead contact upon request. Values for all data points in graphs are reported in the Supporting Data Values file.

Author contributions

K.D.Y. designed and supervised the project. Y.W.C and C.C.L performed the experiments. Y.W.C., L.C, Y.M.L and X.X contributed to data analysis. Y.W.C and C.C.L wrote the original draft. K.D.Y., Z.M.S., and C.C.L. reviewed and edited the manuscript. All authors critically revised the draft and approved the final manuscript.

Acknowledgements

The authors acknowledge funding from the National Key Research and Development Program of China (grant number: 2023YFC3404100/2023YFC3404101 to K.D.Y and C.C.L, 2023YFC2506400 to K.D.Y), and National Natural Science Foundation of China (grant number: 82325042, 82203860, 82072916), and Shanghai Municipal Education Commission Scientific Research Innovation Project (grant number: 2023-05-50), Wu Jieping Medical Foundation Research Project (grant number: 32067502023-18-29). The funders had no role in the study design, data collection and analysis, decision to publish, or preparation of the manuscript.

References

1. Huppert LA, et al. Systemic therapy for hormone receptor-positive/human epidermal growth factor receptor 2-negative early stage and metastatic breast cancer. *CA: a cancer journal for clinicians.* 2023;73(5):480-515.

2. Ma CX, et al. Mechanisms of aromatase inhibitor resistance. *Nature reviews Cancer.* 2015;15(5):261-75.

3. Pan H, et al. 20-Year Risks of Breast-Cancer Recurrence after Stopping Endocrine Therapy at 5 Years. *The New England journal of medicine.* 2017;377(19):1836-46.

4. Dieci MV, et al. Neoadjuvant Chemotherapy and Immunotherapy in Luminal B-like Breast Cancer: Results of the Phase II GIADA Trial. *Clin Cancer Res.* 2022;28(2):308-17.

5. Rugo HS, et al. Safety and Antitumor Activity of Pembrolizumab in Patients with Estrogen Receptor-Positive/Human Epidermal Growth Factor Receptor 2-Negative Advanced Breast Cancer. *Clin Cancer Res.* 2018;24(12):2804-11.

6. Rugo HS, et al. Abemaciclib in combination with pembrolizumab for HR+, HER2- metastatic breast cancer: Phase 1b study. *NPJ Breast Cancer.* 2022;8(1):118.

7. Keenan TE, et al. Molecular correlates of response to eribulin and pembrolizumab in hormone receptor-positive metastatic breast cancer. *Nat Commun.* 2021;12(1):5563.

8. Ozaki Y, et al. Safety and efficacy of nivolumab plus bevacizumab, paclitaxel for HER2-negative metastatic breast cancer: Primary results and biomarker data from a phase 2 trial (WJOG9917B). *Eur J Cancer.* 2022;171:193-202.

9. Nanda R, et al. Effect of Pembrolizumab Plus Neoadjuvant Chemotherapy on Pathologic Complete Response in Women With Early-Stage Breast Cancer: An Analysis of the

Ongoing Phase 2 Adaptively Randomized I-SPY2 Trial. *JAMA Oncol.* 2020;6(5):676-84.

10. Pusztai L, et al. Durvalumab with olaparib and paclitaxel for high-risk HER2-negative stage II/III breast cancer: Results from the adaptively randomized I-SPY2 trial. *Cancer Cell.* 2021;39(7):989-98 e5.

11. Jin X, et al. Molecular classification of hormone receptor-positive HER2-negative breast cancer. *Nature genetics.* 2023;55(10):1696-708.

12. Zhou X, et al. Pharmacologic Activation of p53 Triggers Viral Mimicry Response Thereby Abolishing Tumor Immune Evasion and Promoting Antitumor Immunity. *Cancer Discov.* 2021;11(12):3090-105.

13. Zhu M, et al. Loss of p53 and mutational heterogeneity drives immune resistance in an autochthonous mouse lung cancer model with high tumor mutational burden. *Cancer Cell.* 2023;41(10):1731-48.e8.

14. Ghosh M, et al. p53 engages the cGAS/STING cytosolic DNA sensing pathway for tumor suppression. *Mol Cell.* 2023;83(2):266-80.e6.

15. Hirano T, et al. Dominant negative MEKK1 inhibits survival of pancreatic cancer cells. *Oncogene.* 2002;21(38):5923-8.

16. Kuo SH, et al. MAP3K1 expression is associated with progression and poor prognosis of hormone receptor-positive, HER2-negative early-stage breast cancer. *Cell Oncol (Dordr).* 2023;46(5):1213-34.

17. Liu C, et al. MAP3K1-targeting therapeutic artificial miRNA suppresses the growth and invasion of breast cancer in vivo and in vitro. *Springerplus.* 2016;5:11.

18. Hogquist KA, et al. T cell receptor antagonist peptides induce positive selection. *Cell.*

1994;76(1):17-27.

19. Germann S, et al. Dual role of the ddx5/ddx17 RNA helicases in the control of the pro-migratory NFAT5 transcription factor. *Oncogene.* 2012;31(42):4536-49.

20. Métivier R, et al. Estrogen receptor-alpha directs ordered, cyclical, and combinatorial recruitment of cofactors on a natural target promoter. *Cell.* 2003;115(6):751-63.

21. Ferrari V, et al. Sensitizing cancer cells to immune checkpoint inhibitors by microbiota-mediated upregulation of HLA class I. *Cancer Cell.* 2023;41(10):1717-30.e4.

22. Schmid P, et al. Pembrolizumab for Early Triple-Negative Breast Cancer. *The New England journal of medicine.* 2020;382(9):810-21.

23. Cortes J, et al. Pembrolizumab plus chemotherapy versus placebo plus chemotherapy for previously untreated locally recurrent inoperable or metastatic triple-negative breast cancer (KEYNOTE-355): a randomised, placebo-controlled, double-blind, phase 3 clinical trial. *Lancet.* 2020;396(10265):1817-28.

24. Comprehensive molecular portraits of human breast tumours. *Nature.* 2012;490(7418):61-70.

25. Yujiri T, et al. Role of MEKK1 in cell survival and activation of JNK and ERK pathways defined by targeted gene disruption. *Science.* 1998;282(5395):1911-4.

26. Minamino T, et al. MEKK1 suppresses oxidative stress-induced apoptosis of embryonic stem cell-derived cardiac myocytes. *Proc Natl Acad Sci U S A.* 1999;96(26):15127-32.

27. Cuevas BD, et al. MEKK1 controls matrix degradation and tumor cell dissemination during metastasis of polyoma middle-T driven mammary cancer. *Oncogene.* 2006;25(36):4998-5010.

28. Verma V, et al. MEK inhibition reprograms CD8(+) T lymphocytes into memory stem cells with potent antitumor effects. *Nat Immunol.* 2021;22(1):53-66.

29. Limagne E, et al. MEK inhibition overcomes chemoimmunotherapy resistance by inducing CXCL10 in cancer cells. *Cancer Cell.* 2022;40(2):136-52.e12.

30. Turan T, et al. A balance score between immune stimulatory and suppressive microenvironments identifies mediators of tumour immunity and predicts pan-cancer survival. *Br J Cancer.* 2021;124(4):760-9.

31. Hendrickx W, et al. Identification of genetic determinants of breast cancer immune phenotypes by integrative genome-scale analysis. *Oncoimmunology.* 2017;6(2):e1253654.

32. Bedognetti D, et al. The MAPK hypothesis: immune-regulatory effects of MAPK-pathway genetic dysregulations and implications for breast cancer immunotherapy. *Emerg Top Life Sci.* 2017;1(5):429-45.

33. Seliger B, et al. Coordinate downregulation of multiple MHC class I antigen processing genes in chemical-induced murine tumor cell lines of distinct origin. *Tissue Antigens.* 2000;56(4):327-36.

34. Garrido F, et al. Natural history of HLA expression during tumour development. *Immunol Today.* 1993;14(10):491-9.

35. Marincola FM, et al. Escape of human solid tumors from T-cell recognition: molecular mechanisms and functional significance. *Adv Immunol.* 2000;74:181-273.

36. Garrido F, et al. The urgent need to recover MHC class I in cancers for effective immunotherapy. *Curr Opin Immunol.* 2016;39:44-51.

37. Zhou F. Molecular mechanisms of IFN-gamma to up-regulate MHC class I antigen

processing and presentation. *Int Rev Immunol.* 2009;28(3-4):239-60.

38. Benci JL, et al. Opposing Functions of Interferon Coordinate Adaptive and Innate Immune Responses to Cancer Immune Checkpoint Blockade. *Cell.* 2019;178(4):933-48.e14.

39. Gu SS, et al. Therapeutically Increasing MHC-I Expression Potentiates Immune Checkpoint Blockade. *Cancer Discov.* 2021;11(6):1524-41.

40. Becht E, et al. Estimating the population abundance of tissue-infiltrating immune and stromal cell populations using gene expression. *Genome Biol.* 2016;17(1):218.

41. Charrad M, et al. NbClust: An R Package for Determining the Relevant Number of Clusters in a Data Set. *Journal of Statistical Software.* 2014;061(6):1-36.

42. Reynolds AP, et al. Clustering Rules: A Comparison of Partitioning and Hierarchical Clustering Algorithms. *Journal of Mathematical Modelling & Algorithms.* 2006;5(4):475-504.

43. Newman AM, et al. Robust enumeration of cell subsets from tissue expression profiles. *Nat Methods.* 2015;12(5):453-7.

Figures and Figure Legends

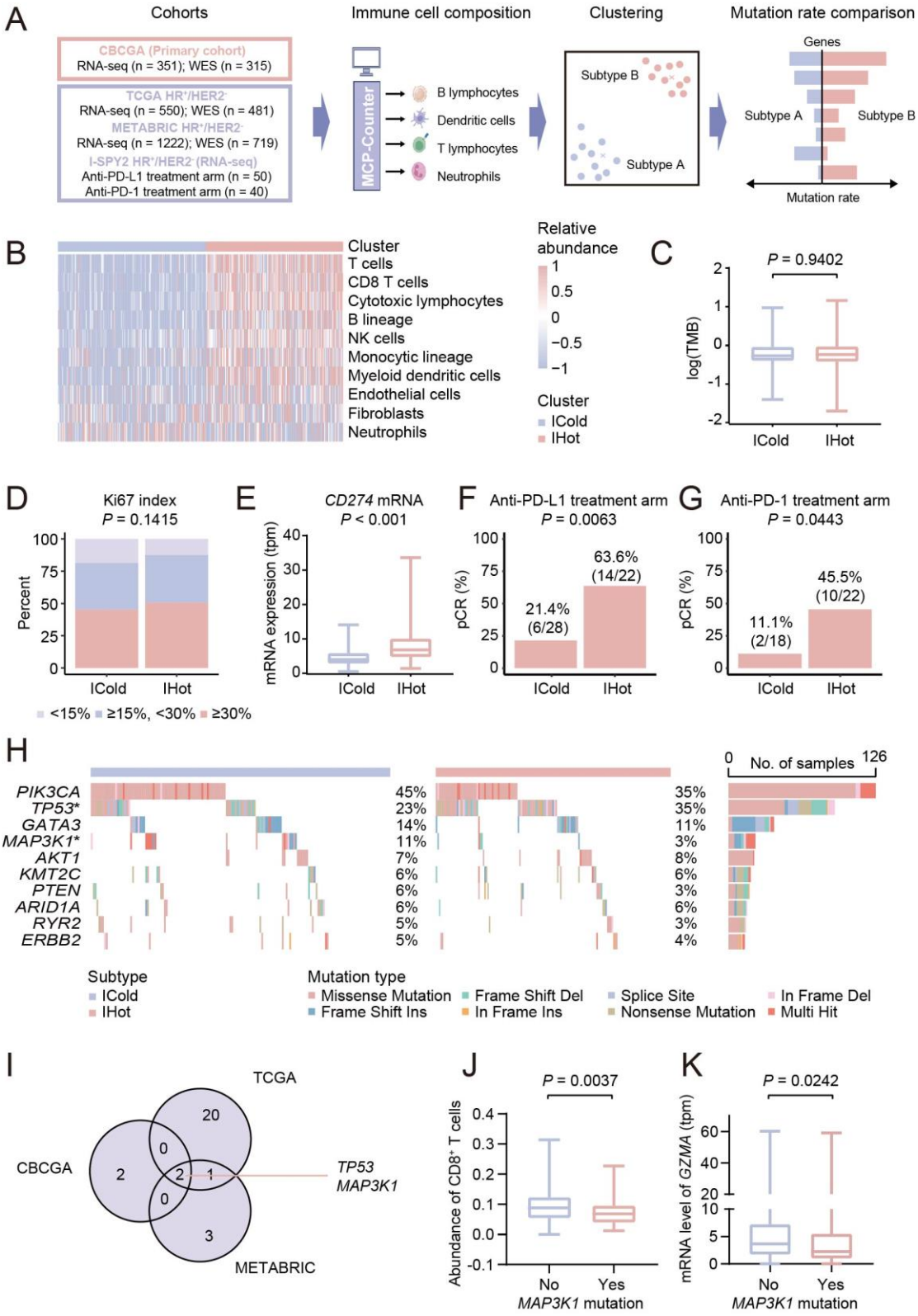

Figure 1. *MAP3K1* mutation is closely correlated with immune microenvironment heterogeneity in HR$^+$/HER2$^-$ breast cancer.

(**A**) Flowchart of bioinformatics analyses performed in the study.

(**B**) Heatmap showing the relative abundance of immune and stromal cells calculated by MCP-Counter in each sample in CBCGA cohort (n = 351). The two immunological subtypes were annotated.

(**C**) Comparison of tumor mutation burden (TMB) of tumors with the ICold and IHot subtypes in CBCGA cohort (n = 314). The center line represents the median.

(**D** and **E**) Comparison of ki67 index (**D**) and *CD274* mRNA expression level (**E**) of tumors with the ICold and IHot subtypes in CBCGA cohort (n = 350). The center line represents the median.

(**F** and **G**) Pathological complete response (pCR) rate of patients with the ICold and IHot subtypes in the anti-PD-L1 (**F**) and anti-PD-1 (**G**) treatment arm of the I-SPY2 clinical trial.

(**H**) The somatic mutations identified in tumors with the ICold and IHot subtypes in CBCGA cohort (n = 314). **P* < 0.05.

(**I**) Venn diagram showing genes with significantly different mutation prevalence between the ICold and IHot subtypes in CBCGA (n = 314), TCGA $HR^+/HER2^-$ (n = 475), and METABRIC $HR^+/HER2^-$ (n = 611) breast cancer cohorts.

(**J** and **K**) Abundance of $CD8^+$ T cells calculated by CIBERSORT (**J**) and *GZMA* mRNA expression (**K**) in $HR^+/HER2^-$ breast tumors with or without *MAP3K1* mutation in the TCGA cohort (n = 481).

Statistical analysis: (**C**, **E**, **J**, and **K**) Wilcoxon signed-rank test; (**D**) chi-square test for trend; (**F**-**H**) Fisher's exact test. ICold, immune cold subtype; IHot, immune hot subtype; TMB, tumor mutation burden; HR, hormone receptor; HER2, human epidermal growth factor receptor 2.

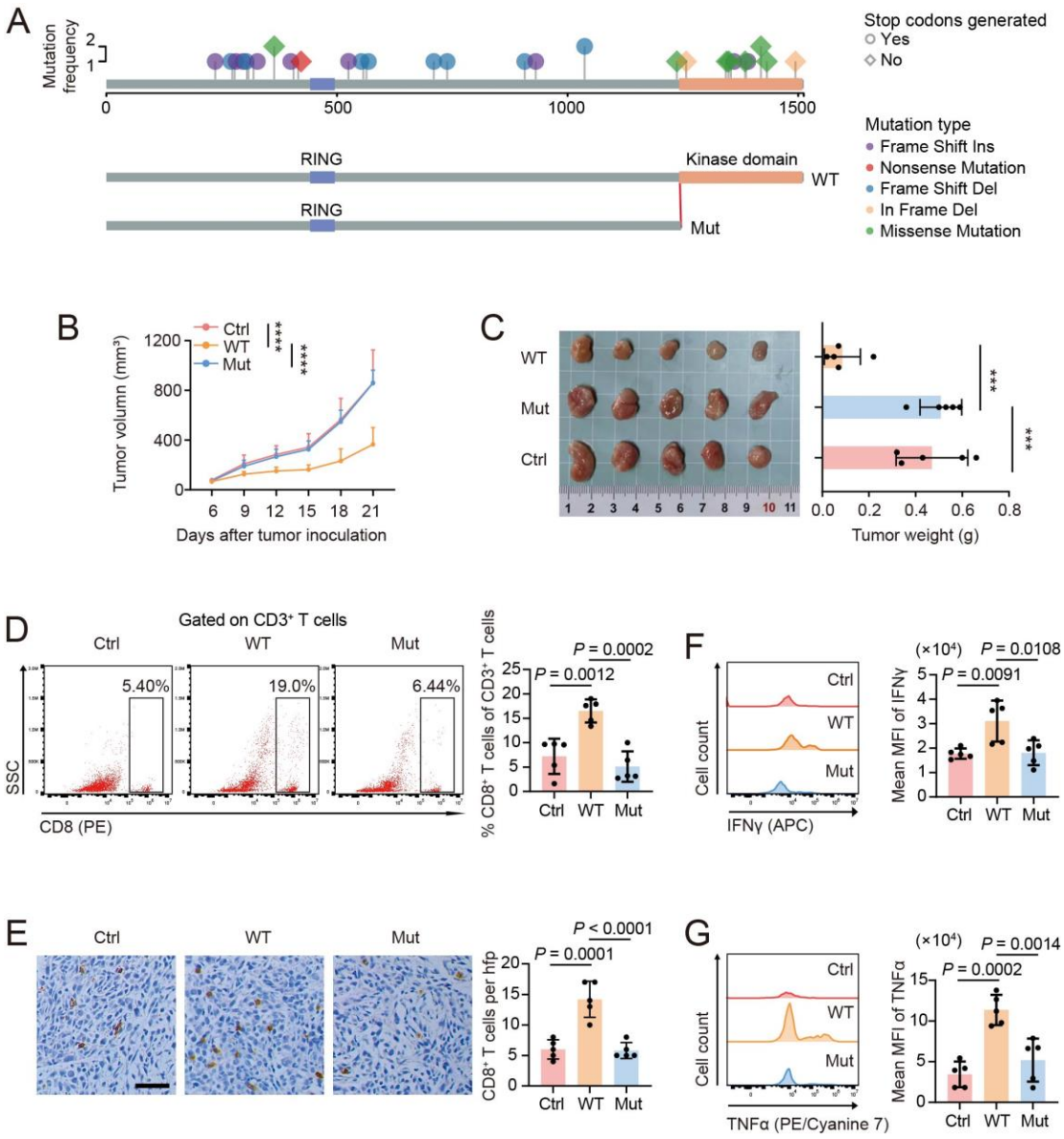

Figure 2. *Map3k1*-mutant tumors evade CD8$^+$ T cell-mediated immunity in vivo.

(**A**) *MAP3K1* mutation atlas of tumors in the CBCGA cohort and schematic diagram of full-length (WT) and kinase domain-truncated (1-1222 aa) *Map3k1* (Mut) overexpression plasmids generated for the following experiments. The mutation type and whether a stop codon was generated are annotated.

(**B** and **C**) 67NR mouse breast cancer cells with varying *Map3k1* status (overexpression based on *Map3k1* KO cell lines) were orthotopically injected into BALB/c mice (n = 5 per group). Tumor growth curves (**B**) and tumor weights with the images (**C**) are shown.

(**D**) Representative flow cytometry data of CD8$^+$ T cell infiltration gated on CD3$^+$ T cells in tumor tissues.

(**E**) Representative IHC images of tumor tissues are shown and the numbers of $CD8^+$ T cell are quantified. Scale bar, 50 μm.

(**F** and **G**) MFI of IFNγ (**F**) and TNFα (**G**) in $CD8^+$ T cells in the tumor tissues.

Data are mean ± SD (**B**-**G**) (n = 5 per group). Statistical analysis: (**B**) two-way ANOVA with Tukey's test; (**C**-**G**) one-way ANOVA with Tukey's test. Significance in tumor growth (**B**) and tumor weight (**C**) data is annotated: $*P < 0.05$, $**P < 0.01$, $***P < 0.001$, $****P < 0.0001$.

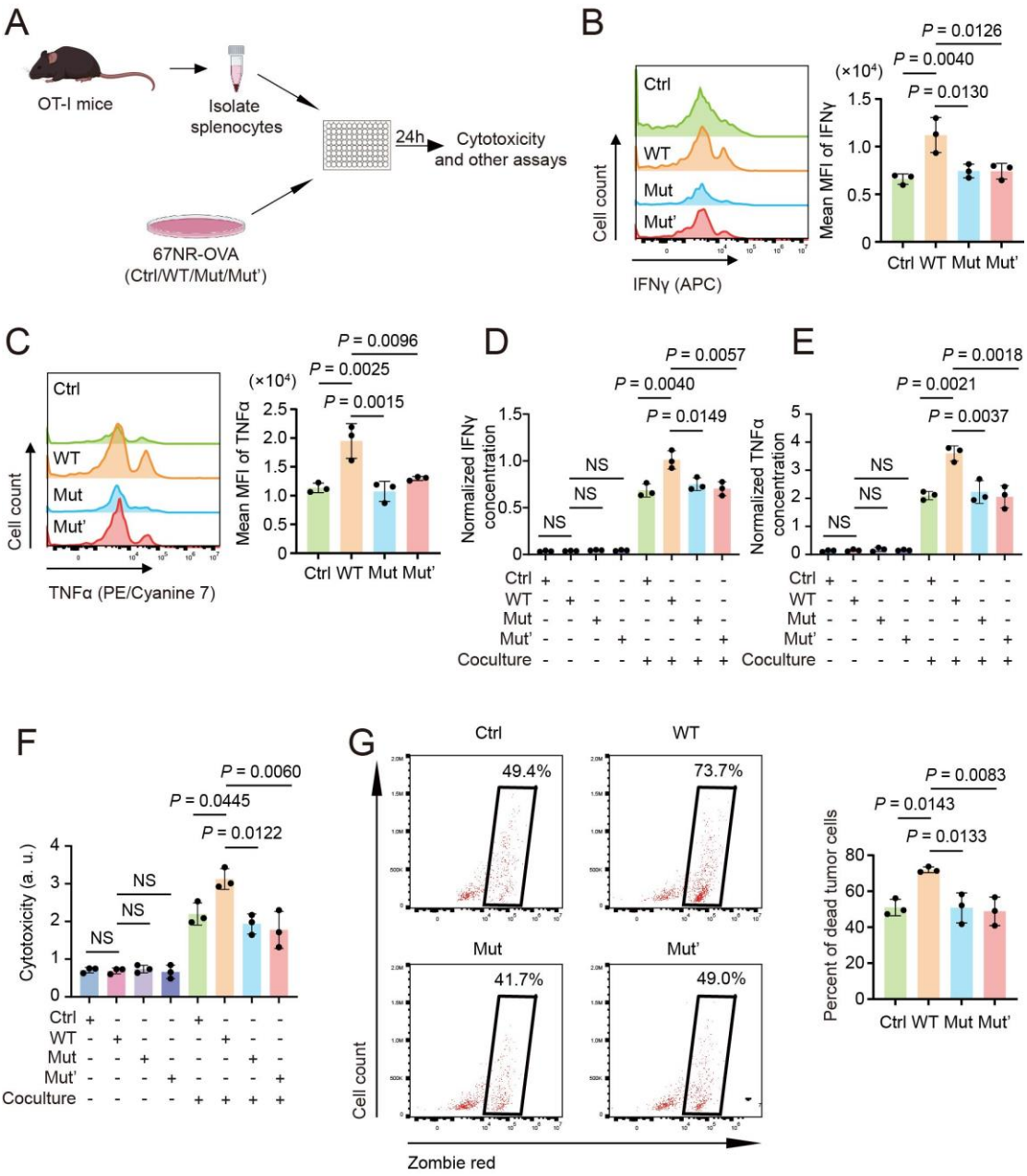

Figure 3. *MAP3K1* mutation inhibits CD8$^+$ T cells activation in vitro.

(**A**) Schematic diagram of the in vitro coculture assay. OVA-expressing 67NR tumor cells with varying *Map3k1* status were cocultured with splenocytes isolated from OT-I mice at a ratio of 1:10. At 24 hours after coculture, tumor cells, immune cells, and the culture medium were collected for the following analyses.

(**B** and **C**) MFI of IFNγ (**B**) and TNFα (**C**) in CD8$^+$ T cells are shown.

(**D** and **E**) Concentration of cytokines IFNγ (**D**) and TNFα (**E**) in the culture medium was measured by ELISA.

(**F**) T cell cytotoxicity was measured by lactate dehydrogenase (LDH) assay.

(**G**) T cell cytotoxicity was assessed by the percentage of dead cells in $EpCAM^+$ tumor cells.

Data are mean ± SD (**B**-**G**) (n = 3 per group). Statistical analysis: (**B**-**G**) one-way ANOVA with Tukey's test.

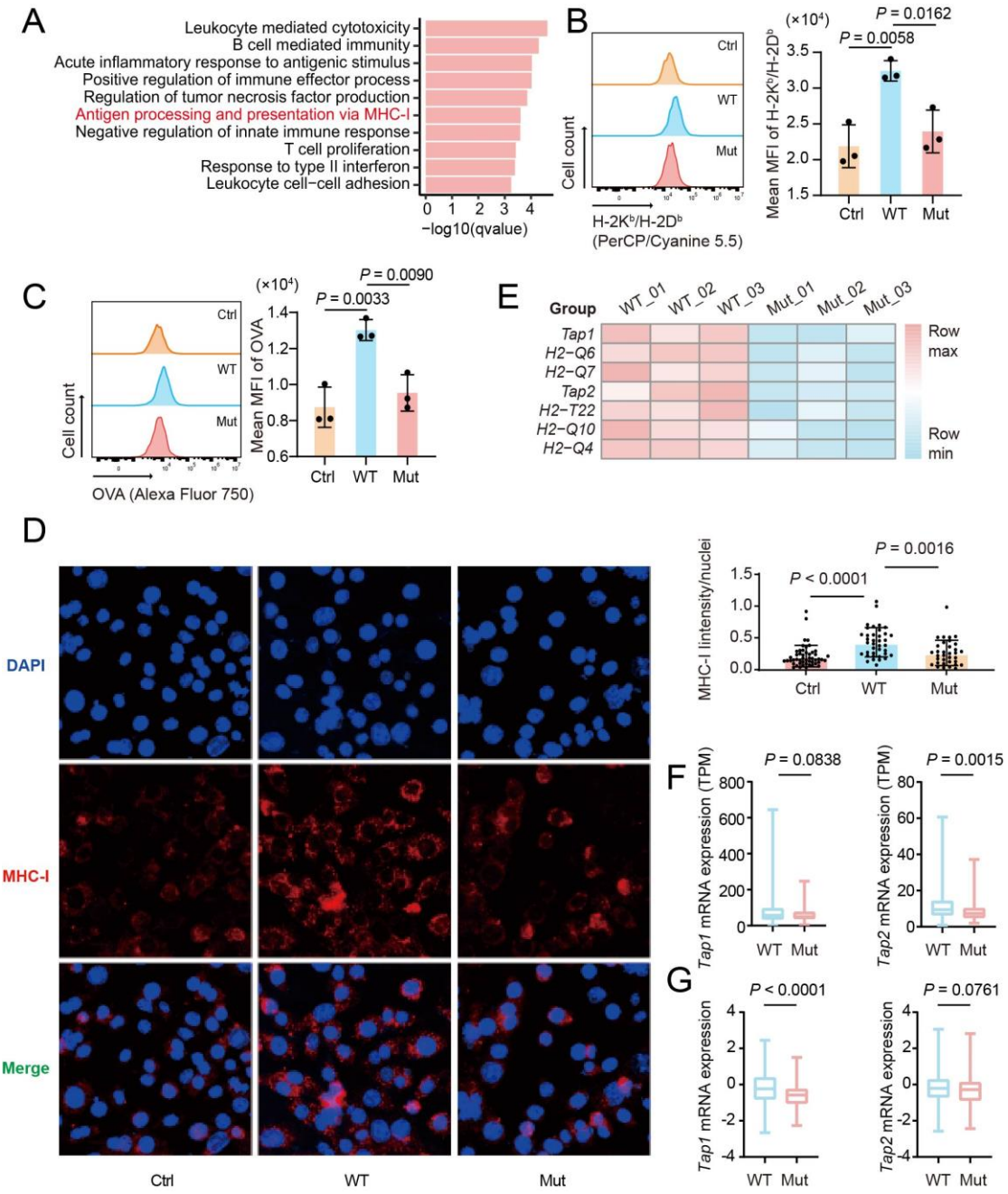

Figure 4. *MAP3K1* mutation suppresses tumor antigen presentation.

(**A**) *Map3k1*-WT and *Map3k1*-Mut tumor tissues were collected for RNA-Seq. GO enrichment analysis was performed and immune-related pathways that are significantly downregulated in *Map3k1*-Mut compared to *Map3k1*-WT tumors are shown here. (n = 3 per group)

(**B** and **C**) Surface expression of H-2K^b/H-2D^b (**B**) and OVA (**C**) on 67NR tumor cells with varying *Map3k1* status after coculture with OT-I splenocytes for 24 hours was determined by flow cytometry.

(**D**) Surface expression of MHC-I on tumor cells in (**B** and **C**) was also measured by immunofluorescence. Scale bar: 50 μm.

(**E**) Heatmap showing the significantly downregulated genes in *Map3k1*-Mut compared to *Map3k1*-WT tumors in the pathway of antigen processing and presentation via MHC-I. Significance determined as *P* value less than 0.05 and fold change less than 0.8.

(**F** and **G**) Comparison of mRNA expression of *Tap1/2* in *MAP3K1*-WT and *MAP3K1*-Mut tumors in TCGA (n = 481) (**F**) and METABRIC (n = 719) (**G**) cohorts. The center line represents the median.

Data are mean ± SD (**B** and **C**) (n = 3 per group). Statisti0cal analysis: (**B**-**D**) one-way ANOVA with Tukey's test. (**F** and **G**) Wilcoxon signed-rank test.

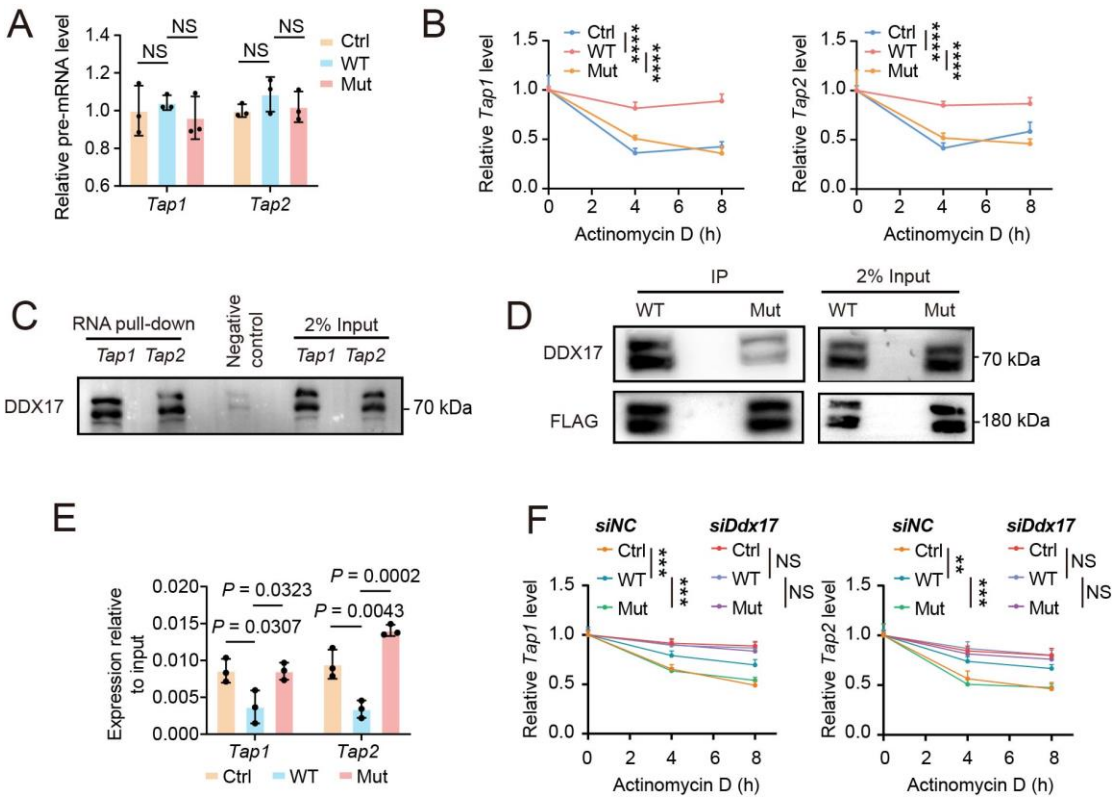

Figure 5. *Map3k1* mutation promotes *Tap1/2* RNAs degradation.

(**A**) The pre-mature mRNA level of *Tap1/2* in 67NR-OVA cells with varying *Map3k1* status in coculture was measured by RT-qPCR.

(**B**) 67NR-OVA cells with varying *Map3k1* status were cocultured with OT-I splenocytes for 24 hours and then treated with actinomycin D at a dose of 10 μg/ml. Tumor cells were collected at the indicated time points to perform RT-qPCR to test the RNA level of *Tap1/2*.

(**C**) RNA pull-down assay was performed to examine the binding of *Tap1/2* mRNAs to DDX17 in 67NR-OVA cells in coculture.

(**D**) IP assay was performed to examine and compare the binding of *Map3k1*-WT and *Map3k1*-Mut to DDX17 in 67NR-OVA cells in coculture.

(**E**) 67NR-OVA cells with varying *Map3k1* status in coculture were collected and RNA immunoprecipitation (RIP) assay was performed to extract the RNA binding to DDX17. RT-qPCR was then performed to measure the RNA levels of *Tap1/2*.

(**F**) 67NR-OVA cells with varying *Map3k1* status were transiently transfected with small interfering RNA targeting *Ddx17* (*siDdx17*) or its control RNA (*siNC*). One day

after transfection, tumor cells were cocultured with OT-I splenocytes for 24 hours and then treated with actinomycin D at a dose of 10 μg/ml. Tumor cells were collected at the indicated time points and RT-qPCR was performed to test the RNA level of *Tap1/2*. Data are mean ± SD (**A**, **B**, **E**, and **F**) (n = 3 per group). Statistical analysis: (**A** and **E**) one-way ANOVA with Tukey's test. (**B** and **F**) two-way ANOVA with Tukey's test. Significance in the RNA degradation experiments (**B** and **F**) is annotated: $*P < 0.05$, $**P < 0.01$, $***P < 0.001$, $****P < 0.0001$.

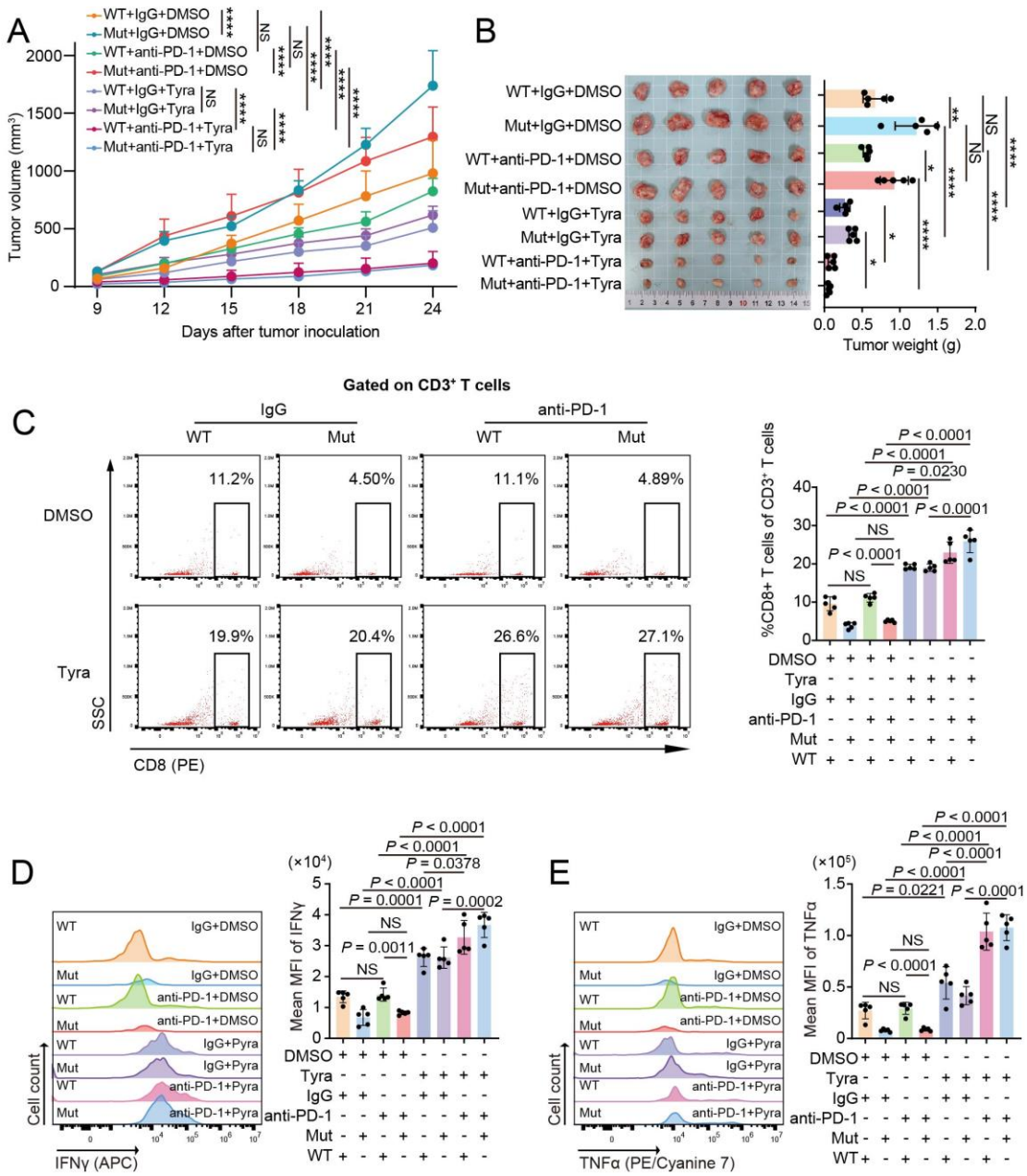

Figure 6. Tyramine augments the efficacy of immunotherapy in HR$^+$/HER2$^-$ breast cancer.

(**A** and **B**) 67NR cells expressing *Map3k1*-WT or *Map3k1*-Mut were orthotopically injected into BALB/c mice. Once tumors formed, mice were randomly assigned to receive tyramine (Tyra) or DMSO in combination with anti-PD-1 or its isotype control (IgG). Tumor growth curves (**A**) and tumor weights with the images (**B**) are shown here. (**C**) Representative flow cytometry data of CD8$^+$ T cell infiltration in tumor tissues. (**D** and **E**) MFI of IFNγ (**D**) and TNFα (**E**) in CD8$^+$ T cells in the tumor tissues. Data are mean ± SD (**A**-**E**) (n = 5 per group). Statistical analysis: (**A**) two-way ANOVA

with Tukey's test; (**B**-**E**) one-way ANOVA with Tukey's test. Tyra, tyramine. HR, hormone receptor; HER2, human epidermal growth factor receptor 2.